Noname manuscript No.
(will be inserted by the editor)

MODELING AND CONTROL OF A FINGER-LIKE MECHANISM USING BENDING SHAPE MEMORY ALLOYS

Hussein F. M. Ali, Abdul Manan Khan, Hangyeol Baek, Bu Hyun Shin, and Youngshik Kim

the date of receipt and acceptance should be inserted later

Abstract In this research a biologically inspired finger-like mechanism similar to human musculoskeletal system is developed based on Shape Memory Alloys (SMAs). SMA actuators are inspiring the design of a modular finger part with compact and compliant actuation. A three-segmented finger-like mechanism is designed and fabricated. This mechanism is composed of six bending Shape Memory Alloy (SMA) actuators. As a result, our finger mechanism is compact and compliant. The insider three SMA actuators are used for finger flexion while the outsider three SMA actuators are for extension. Each segment of this mechanism can be bent and/or extended independently by actuating a corresponding bending SMA actuator. Furthermore, full bending motion can be achieved by applying coordinated control of the three SMA actuators. Toward this goal a mathematical model of the SMA combined finger has been developed. The developed mathematical model is then used to design a proportional-derivative (PD) controller for control compliant actuation of the finger-mechanism. The performance of this mechanism has been experimentally evaluated. Our experimental results verify that the SMA-based finger module can achieve the desired postures similar to a human finger.

Hussein F. M. Ali, E-mail: hussein.ali@ejust.edu.eg
Mechanical Engineering, Benha University, Benha, Egypt
Current Address: Mechanical Engineering, Hanbat National University, Daejeon, S. Korea

Abdul Manan Khan, E-mail: abdul.mannan.617@gmail.com
Mechanical Engineering, Hanbat National University, Daejeon, South Korea

Hangyeol Baek, E-mail: dmb03085@naver.com
Electronics and Control Engineering, Hanbat National University, Daejeon, South Korea

Bu Hyun Shin, E-mail: jedidiah@hanbat.ac.kr
Mechanical Engineering, Hanbat National University, Daejeon, South Korea

Corresponding Author: Youngshik Kim, E-mail: youngshik@hanbat.ac.kr
Department of Mechanical Engineering, Hanbat National University, Yuseung-gu Dukmyung-dong San 16-1, Building: N7-407, Daejeon 305-719, South Korea.

Keywords artificial finger · coordinated control · compliance · shape memory alloy actuator · soft robot

1 Introduction

In recent years, smart materials are used in various areas in bio-medical applications. One group of these materials is the Shape Memory Alloys (SMAs). The main advantages of SMAs are: noiseless actuation, compact size, high force to weight ratio, and high density work Jani et al. (2014); Langbein (2009). These properties have enabled SMAs to be used as smart and compliant actuators for many applications ranging from small bio-inspired robots to aerospace.

In this study, we are focusing on robotic actuators using SMAs. There have been many different kinds of robotic applications. Mainly they are categorized as walking (Peng et al. (2020); Mao et al. (2019)), swimming (Almubarak et al. (2020); Song et al. (2016)) and grasping robots (Lee et al. (2019a); Maffiodo and Raparelli (2019); Lu et al. (2019)). They are mainly being used for having compliant and soft actuation. As compared to other robotic actuators like electric, hydraulic or pneumatic, SMA actuators do not need complicated mechanical appendages for power transmission. They are attached with the structure of the body like musculoskeletal system. These properties have made SMAs very suitable particularly for soft grippers.

For the SMA applications, in grippers, there have been significant research (Tai et al. (2016); Wang and Ahn (2017); Wang et al. (2016)). As soft actuation can give compliant grasping, many authors have developed different kinds of robotic grippers using SMAs (Rodrigue et al. (2017); Simone et al. (2017); Lee et al. (2019b)). Mainly, the design can be categorized as 1) human finger like joint structures (Wang et al. (2020b); Ades et al. (2020); Simone et al. (2019)), 2) continuous flexible type structures (Wang et al. (2020a); Liu et al. (2020); Lee et al. (2019b)). The main advantage of continuous flexible type structures is that the finger angles take the complex shape of an object, even though it is difficult to control the angles to certain values. On the other hand, for human finger like joint structures it is possible to control the angles (DeLaurentis et al. (2000); Laurentis and Mavroidis (2002); Andrianesis and Tzes (2015); Bundhoo et al. (2009); Gilardi et al. (2010); Ali et al. (2020)). Maffiodo and Raparelli (2019) have developed four flexible fingers based on SMA actuation modules. Lee et al. (2019a) have developed long SMA tendon-based soft robotic actuators and implementation as a soft gripper. DeLaurentis et al. (2000); Laurentis and Mavroidis (2002) developed a robotic hand using SMAs for human finger like structures for prosthetic hand.

In the research conducted by DeLaurentis et al. (2000); Laurentis and Mavroidis (2002); Andrianesis and Tzes (2015); Bundhoo et al. (2009); Gilardi et al. (2010) only open loop control was implemented. Their focus was on manufacturing and design. We, Ali et al. (2020), have also developed open loop control of the present SMA actuated robotic finger in our previous stage. However, we need closed loop control to grasp complex shaped objects and for

prosthetic hand applications. It is difficult to grasp a complex shaped objects using open loop control system. For example, Lee et al. (2019b) compliant motion has been discussed and many objects have been shown to grasp by the finger. However, only open loop control is implemented in most of these studies. Based on that, for grasping feedback control will be useful.

To develop a closed loop control of SMA actuated robotic hand, we need to model the dynamics of SMA. There have been many different methods to model the dynamics of SMAs. The prominent methods are developed by Tanaka (1986) Tanaka (1986), Liang et. al. (1990) Liang and Rogers (1997), Brinson et. al. (1993)Brinson (1993) and Elahinia et. al. (2005)Elahinia and Ahmadian (2005). All the methods were continuity of its predecessors with gradual improvements. Elahinia et. al.Elahinia and Ahmadian (2005) combined the stress, strain and temperature relation in its model which were separately considered by the other previous authors. Therefore, we have adopted Elahinia et. al.'s method to model the dynamics of SMA for our study.

In this paper, we have presented a novel robotic finger design which is based on curved SMA wires. Curved SMA wires generate rotary motion (there is no need to attach circular disk to transform linear motion into rotary motion for the robotic finger). The proposed novel biologically inspired robotic finger is composed of three segmented SMA actuators similar to human musculoskeletal system. Furthermore, to control the SMA actuated finger, we have modeled the SMAs using Elahinia and Ahmadian (2005) method. This dynamic modeling of SMA is used to design and tune the proportional-derivative controller for the finger. We have conducted experiments to demonstrate the effectiveness of closed loop control and curved shaped SMA actuators for the novel robotic finger. Experimental results confirm the successful regulation of the desired angles by SMAs.

2 SMA ACTUATION UNIT

The main idea of the SMA actuation is based on the thermo-mechanical properties of an SMA as the change of the deformed material state (from Martensite to Austenite) when heated, and hence the SMA restores the original shape of the straight wire. When the SMA is cooled, it will return to the Martensite state again while keeping its original shape, as shown in Fig.1. A single actuator unit is composed of one array of the deformed SMA wire in an arc shape below the transient temperature, Table 1. This wire is welded to two PCB supporting elements as shown in Fig.2. The displacement angle, $\theta \cong 0$ when the SMA is deformed by loading at room temperature, state 1 (Martensite). The displacement is θ_{max} when heated, state 2 (Austenite). When the SMA is cooled to the room temperature, it becomes the state 3 (Martensite). As a result, this SMA actuator can provide torque through heating the wire array by applying electrical power. This SMA actuator gives rotational motion similar to the revolute joint with angle ($0 < \theta < \theta_{max}$).

In this study, a modular bending actuator is constructed using an actuating unit in wire array to form 10 arcs as shown in Fig. 2. Antagonistic pairs are designed to extend the finger in the opposing direction as shown in Fig.3. Three actuator units (flexion type) are then serially connected to map the three DOF of the human finger as shown in Fig.4. Each link (Distal, Middle, and Proximal) is attached separately to an antagonistic SMA units similar to that in Fig.3. An elastic string is used to initially pose the finger mechanism straight.

3 SMA ACTUATOR CHARACTERIZATION

This section presents experimental characterization of the single module actuator, which will provide the essential parameters understanding for the actuator control in next sections.Especially, spring constants, mechanical responses, thermal responses, and resulting temperature of SMA for several different electrical power inputs.

3.1 Mechanical Characterization

The spring constant of the actuator is investigated. Two cases are considered to find the spring constant of the SMA actuator when increasing and decreasing the actuator displacement. These experiments are repeated at various temperatures to realize the material behavior when controlling the temperature

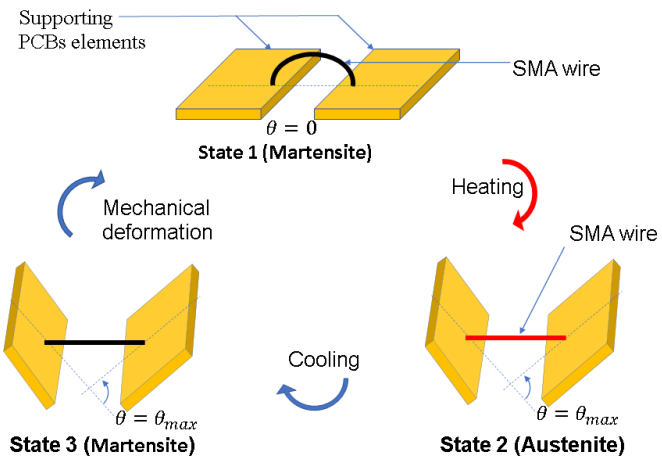

Fig. 1: Bending SMA actuator and its thermo-mechanical states. Actuator states classification: State1 (Martensite; cold deformation), State2 (Austenite; when heated), and State3 (Martensite; when cooled)

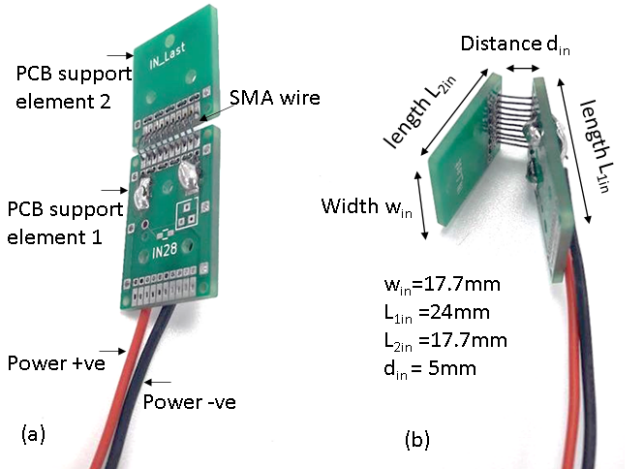

Fig. 2: Bending actuator prototype using an SMA wire actuation unit (for finger flexion). 10 arcs wire is in the array form and two PCB supporting elements: (a) State1 (deformed) and (b) State2 (heated).

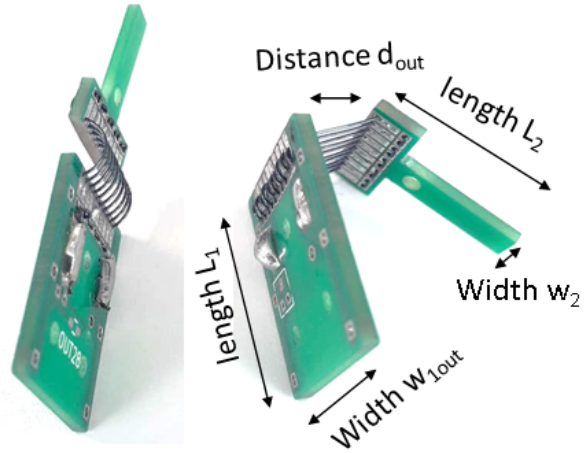

Fig. 3: Antagonistic bending actuator prototype using SMA wire actuation unit (for finger extension)

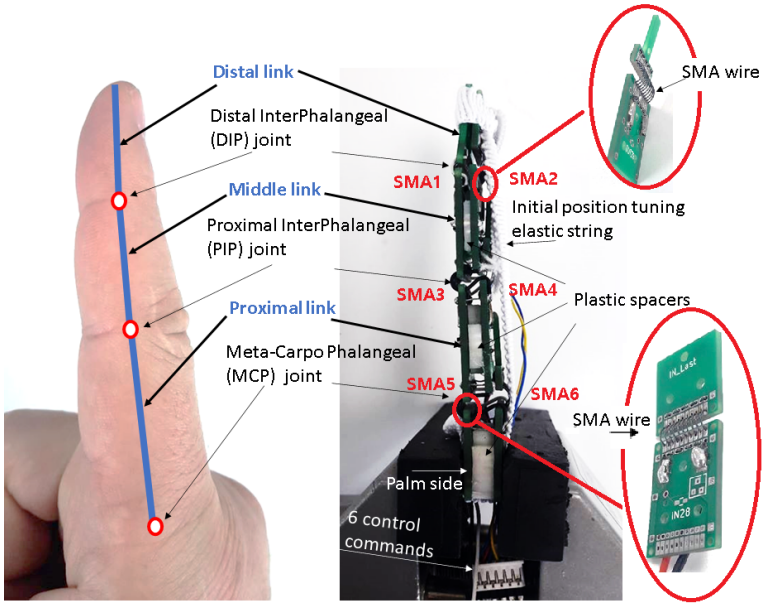

Fig. 4: Human finger versus the finger-like mechanism with 6 SMA actuators. (the inner 3 for bending and the outer 3 for extension)

changes.The experimental setup is shown in Fig.5. The SMA actuator module (1) is clamped with the bench vise. As an input, the force sensor holder (2) moves step by step (from 1 to 11 mm) in the x-direction using the micrometer device. The protractor (3) reads the SMA actuator deflection angle. The PW4MC3 force sensor (4) contacts with the PCB supporting element. The force reading is amplified using amplifier STT-100 (5) and acquired using the Data acquisition NI USB-6009 (6). The amplified force sensor voltage is correlated to the force and finally the moment using equations (1) and (2). The moment versus angle correlation at various temperatures (at room temperature, 40°C, and 70°C) are shown in Fig.6. The spring constant is 59.34 mNm/rad when the angle is increasing and it is 51 mNm/rad when it is decreasing. It is clear that for certain angle, the output moment is almost duplicated at 70°C when compared to that at room temperature.

$$F = 0.292V_m - 0.102 \quad (Newton) \tag{1}$$

$$M = F \times r = F \times 16 \quad (m\ Nm) \tag{2}$$

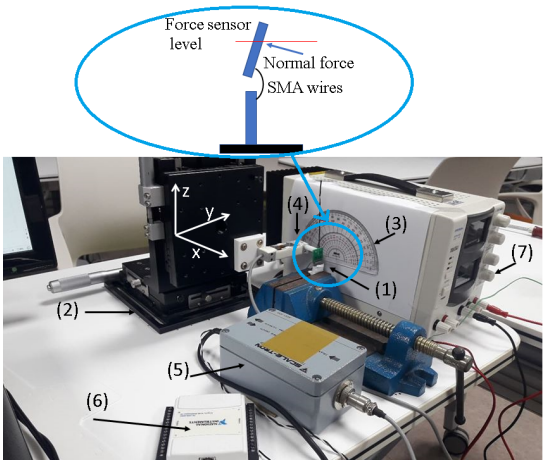

Fig. 5: Experimental Setup for SMA Actuator Characterization.

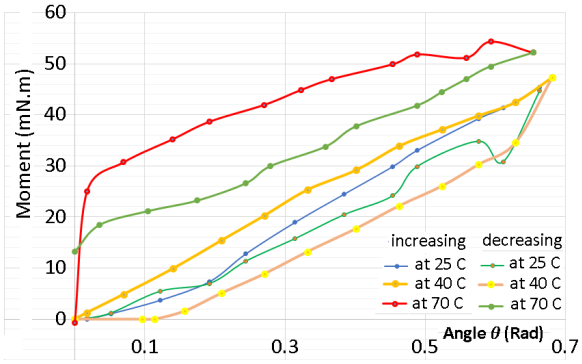

Fig. 6: Moment versus angle of the SMA actuator at room temperature 25 $C°$, 40°C, and 70°C.

3.2 Thermal Characterization

The thermal characteristics is studied at various electrical power input. The temperature of SMA will keep increasing almost linearly when increasing the power as shown in Fig.7(a). It should not exceed 90° Celsius to prevent physical damages to the SMA. The moment is also measured for the same applied power, Fig.7(b). It is noticed that the moment increases non-linearly and tends to saturate at maximum moment of 30 mNm. The same experiment is repeated to measure the angular displacement, Fig.7(c). It increases non-linearly and tends to saturate at maximum angle of 1.6 rad.

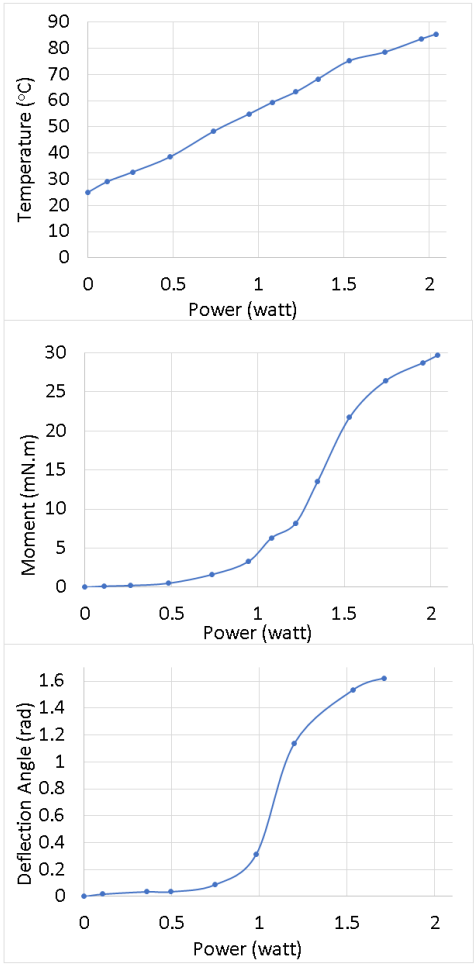

Fig. 7: Thermal and mechanical characterization as a function of the electrical input power.

4 Modeling and Control SMA Finger System

The finger-like mechanism, Fig. 4, is constructed using the two SMA actuator pairs, Fig.2 and Fig.3. The inner 3 SMA actuators (SMA1, SMA3, and SMA5) are for bending and the outer 3 antagonistic SMA actuators (SMA2, SMA4, and SMA6) are for extension. Each joint can be bended/retracted to an angle of 90° from 0° depending on the power applied to the SMA actuator.

4.1 Kinematic Modeling of Finger

Considering kinematics of the SMA finger, we can easily determine positions of each joint and the end effort point by,

$$x_1 = L_1 \cos(\theta_1), \quad y_1 = L_1 \sin(\theta_1) \tag{3}$$
$$x_2 = L_1 \cos(\theta_1) + L_2 \cos(\theta_{12}), \tag{4}$$
$$y_2 = L_1 \sin(\theta_1) + L_2 \sin(\theta_{1,2}) \tag{5}$$
$$x_3 = L_1 \cos(\theta_1) + L_2 \cos(\theta_{12}) + L_3 \cos(\theta_{123}) \tag{6}$$
$$y_4 = L_1 \sin(\theta_1) + L_2 \sin(\theta_{12}) + L_3 \sin(\theta_{123}) \tag{7}$$

where $(x_{i-1}\ ,\ y_{i-1})$ represents the position of i^{th} joint in the reference frame XY (i= 1, 2, 3). θ_i is the angle of joint i and L_i is the length of link i. x_3 and y_3 represent the position of the end effector. Further, $\theta_{12} = \theta_1 + \theta_2$, and $\theta_{123} = \theta_1 + \theta_2 + \theta_3$. Using Eq. (3), the workspace of the finger is analyzed in Fig.8.

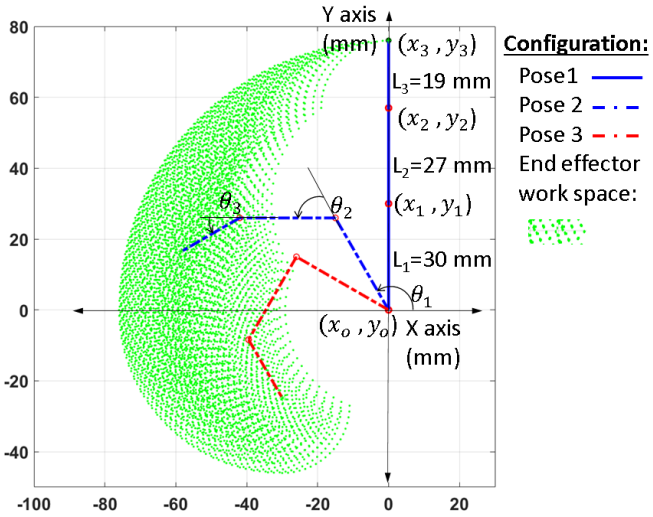

Fig. 8: Work space of the 3-DOF SMA finger like mechanism

4.2 SMA Modeling

4.2.1 Constitutive Model

The constitutive model of SMA is based on Elahinia and Ahmadian (2005) model. The constitutive model of SMA can be described as a relation of stress σ, temperature T, strain ϵ and martensite fraction ξ as

$$\dot{\sigma} = E\dot{\epsilon} + \Omega\dot{\xi} + \Theta\dot{T} \tag{8}$$

where $\dot{(\ )}$ represents time derivative of the concerned quantity, E is Young's modulus, Ω is a transformation tensor and Θ is a thermoelastic tensor.

4.2.2 Martensite Fraction Model

Furthermore, conversion of martensite fraction ξ from martensite state to austenite state shows hysteresis phenomenon. $\xi = 1$ implies that SMA is in martensite state (cold), and $\xi = 0$ means that SMA is completely in austenite state (hot) state. This conversion (from martensite to austenite state) produce stress in SMAs. This conversion is a combination of loading ($\dot{\sigma}$) and heating ($\dot{T}$) and can be represented as, Elahinia and Ahmadian (2005):

$$\dot{\xi} = \xi_T(T,\sigma)\dot{T} + \xi_\sigma(T,\sigma)\dot{\sigma}. \tag{9}$$

Here, ξ_T and ξ_σ are given by

$$\xi_T(T,\sigma) = \begin{cases} \text{if } A_s < T_A < T_f \text{ and } \dot{T}_A > 0 \\ \frac{-\xi_M}{2}\sin(a_A(T_A - A_s))a_A, \\ \\ \text{if } M_f < T_M < M_s \text{ and } \dot{T}_M < 0 \\ \frac{1-\xi_A}{2}\sin(a_M(T_M - M_f))a_M, \\ \\ 0, \qquad\qquad\qquad\qquad \text{otherwise} \end{cases} \tag{10}$$

$$\xi_\sigma(T,\sigma) = \begin{cases} \text{if } A_s < T_A < T_f \text{ and } \dot{T}_A > 0 \\ \frac{-\xi_M}{2}\sin(a_A(T_A - A_s))b_A, \\ \\ \text{if } M_f < T_M < M_s \text{ and } \dot{T}_M < 0 \\ \frac{1-\xi_A}{2}\sin(a_M(T_M - M_f))b_M, \\ \\ 0 \qquad\qquad\qquad\qquad \text{otherwise.} \end{cases} \tag{11}$$

where $T_A = T - \frac{\sigma}{C_A}$ and $T_M = T - \frac{\sigma}{C_M}$. A_s and M_s are the temperatures at which SMA starts converting into austenite and martensite states, respectively.

Table 1: Flexinol (NiTi) SMA Parameters

Parameter	Definition	Value	Unit
M_s	Martensite start temperature	72	°C
M_f	Martensite final temperature	62	°C
A_s	Austenite start temperature	88	°C
A_f	Austenite final temperature	98	°C
C_A	Austenite stress-influence coefficient	10	MPa °C^{-1}
C_M	Martensite stress-influence coefficient	10	MPa °C^{-1}
E_A	Austenite Young modulus	75	GPa
E_M	Martensite Young modulus	28	GPa
R_A	Austenite wire resistance	100	μΩ cm
R_M	Martensite wire resistance	80	μΩ cm
Θ_A	Austenite thermal expansion coefficient	11	μ Pa °C^{-1}
Θ_M	Martensite thermal expansion coefficient	6.6	μPa °C^{-1}
σ_s^{cr}	Detwinning start stress	25	MPa
σ_f^{cr}	Detwinning finish stress	78	MPa
ε_L	Maximum recoverable strain	4.1	%
D	SMA wire diameter	0.254	mm
C_p	Thermal capacity of SMA wire	2.046	MJ m^{-3} °C

Note that, all the SMA parameters used in this study are shown in Table 1. A_s occurs while heating and M_s occurs at cooling. Similarly, A_f and M_f are the temperatures at which the austenite and martensite transformation is finished. Furthermore, b_A, b_M, C_A, C_M are constants. These constants are defined as

$$a_A := \pi/(A_f - A_s) \tag{12}$$
$$b_A := -a_A/C_A \tag{13}$$
$$a_M := \pi/(M_s - M_f) \tag{14}$$
$$b_M := -a_M/C_M \tag{15}$$
$$T_A := T - \sigma/C_A \tag{16}$$
$$T_M := T - \sigma/C_M. \tag{17}$$

4.2.3 Heat Transfer Model

SMAs can be heated by supplying electric current. This electrical heating can be represented as, Elahinia and Ahmadian (2005)

$$\dot{T} = \frac{Ri^2}{m_w C_p} - \frac{h_c A_c (T - T_a)}{m_w C_p} \tag{18}$$

where $\dot{T}$ represents rate of change of temperature in degree Celsius per second, C_p represents the specific heat constant, $m_w = 6.8 \times 10^{-4}$ Kg/m is the mass per unit length, i is the applied current, $R = 18.4$ Ohm/m is the resistance per unit length of SMA wires, and $T_a = 25\ C^\circ$ is the ambient temperature. Furthermore, h_c is the coefficient of heat convection, and A_c is the circumference area (exposed for heat exchange) of wire. h_c can be defined as

$$h_c := h_0 + h_2 T^2 \tag{19}$$

where $h_0 = 120$ and $h_2 = 0.001$ are constants. A_c can be calculated as

$$A_c := 2\pi r_s l_0 \tag{20}$$

where $r_s = 1.27 \times 10^{-4}$ m is the cross sectional radius, and $l_0 = 20 \times 10^{-3}$ m is the length of SMA wire. Defining, $\alpha := R/(m_w C_p)$ and $\beta := h_c A_c/(m_w C_p)$, $T_e = T - T_a$, we can represent equation (18) as

$$\dot{T}_e = -\beta T_e + \alpha i^2 \tag{21}$$

4.2.4 Series Elastic Actuator (SEA) Model

In the study, we have used curvy antagonistic configuration of SMA wires. This configuration consists of two sets of SMA wires in which one set of SMA wires is heated while the other set is kept cool. This configuration is shown in Fig. 3. Antagonistic configuration has control on two sides. Having this configuration, we can represent joint dynamics as

$$\ddot{\theta}_j = \sigma_{j_i} A r_{j_i} - \sigma_{j_o} A r_{j_o}; \text{for } j = 1, 2, 3. \tag{22}$$

where σ_{j_i} is the stress caused by SMA wire attached to the inner side (for flexion motion), r_{j_i} is the radius of SMA wires attached to the outer side, A is the cross sectional area, σ_{j_o} is the stress caused by SMA wires attached to the outer side (for extension motion), and r_{j_o} is the radius of the wire attached to the outer side.

Furthermore, we can represent rate of change in strain for the SMA wires attached on the upper $\dot{\epsilon}_{j_u}$ and lower $\dot{\epsilon}_{j_l}$ side of the joint joint j as

$$\begin{aligned} \dot{\epsilon}_{j_i} &= -r_{w_{j_i}} \dot{\theta}_j / l_{0_j} \\ \dot{\epsilon}_{j_o} &= -\dot{\epsilon}_{j_i} \quad \text{for } j = 1, 2, 3. \end{aligned} \tag{23}$$

where $r_{w_j} = 15 \times 10^{-3}$ m is the radius, θ_j is the joint angle, $l_{0_j} = 35 \times 10^{-3}$ m is the initial length of SMA wire.

Combining equation (8) with (18), (21) and (23), we get

$$\dot{\sigma}_{j_i} = f_{j_i}(\dot{\theta}, T, \sigma) + g_{j_i}(T, \sigma) i_{j_i}^2 \tag{24}$$

where

$$f_{j_i}(\dot{\theta}, T, \sigma) = \frac{-r_w \dot{\theta}_j E / l_{0_i} - \beta_i T_{e_{j_i}} (\Omega \xi_T(T_{j_i}, \sigma_{j_i}) + \Theta)}{1 - \Omega \xi_\sigma(T_{j_i}, \sigma_{j_i})} \tag{25}$$

$$g_{j_i}(T, \sigma) = \frac{\Omega \xi_T(T_{j_i}, \sigma_{j_i}) + \Theta}{1 - \Omega \xi_\sigma(T_{j_i}, \sigma_{j_i})} \alpha_i. \tag{26}$$

For the SMA attached to the outer side of joint j, we can write

$$\dot{\sigma}_{j_o} = f_{j_o}(\dot{\theta}, T, \sigma) + g_{j_o}(T, \sigma) i_{j_o}^2 \tag{27}$$

where

$$f_{j_o}(\dot{\theta}, T, \sigma) = \frac{-r_w \dot{\theta}_j E / l_{0_j} - \beta_o T_{e_{j_o}} (\Omega \xi_T(T_{j_o}, \sigma_{j_o}) + \Theta)}{1 - \Omega \xi_\sigma(T_{j_o}, \sigma_{j_o})} \tag{28}$$

$$g_{j_o}(T, \sigma) = \frac{\Omega \xi_T(T_{j_o}, \sigma_{j_o}) + \Theta}{1 - \Omega \xi_\sigma(T_{j_o}, \sigma_{j_o})} \alpha_o. \tag{29}$$

All the parameters for the used SMA are given in Table 1.

4.3 Independent Joint Control PD

SMAs are attached at each join in antagonistic configuration. For this study, we have used independent joint control for 3-DOF robotic finger. For this purpose, we have used proportional-derivative (PD) controller to regulate the joint angles. To achieve this objective, we determined different control gains for each actuator using the SMA model presented in Section 4.1. There was difference in the gains obtained in simulation and experiment.

The independent PD controller generates the current signal to actuate concerned SMA. PD control law for independent joint control is as follows:

$$C_{PD} = P_j(\theta_j - \theta_{j_D}) + D_j\left(\dot{\theta}_j - \dot{\theta}_{j_D}\right) \quad \text{for} \quad j = 1, 2, 3. \tag{30}$$

where P_j, D_j are proportional and derivative gains for the joint j. In the same way, θ_j and θ_{j_D} represent the actual and desired angle for the joint j.

Furthermore, if $C_{PD} \geq 0 \rightarrow i_1 = C_{PD}, i_2 = 0$, inner SMA (for joint 3, SMA-1) is actuated and outer SMA (for joint 3, SMA-2) is kept at 0. if $C_{PD} \leq 0 \rightarrow i_1 = 0, i_2 = C_{PD}$, outer SMA (SMA-2) is actuated keeping the inner SMA (SMA-1) at 0.

For safety, we have imposed temperature limitations in the controller. The upper limit of temperature for both the SMAs is 110° Celsius to prevent permanent deformation of SMA.

The block diagram of physical and simulation system with controller is shown in Fig. 9. In this figure, θ is the feedback which is compared with the desired angle θ_D. The error between desired angle θ_D and system angle θ is fed

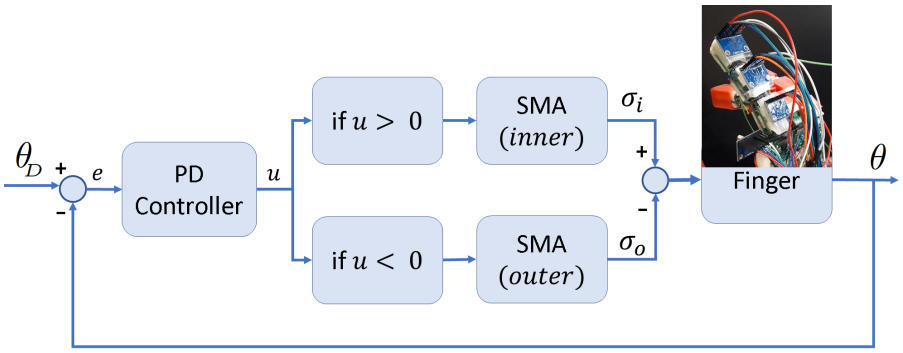

Fig. 9: PD Controller Block Diagram where u is the control effort, e is the error signal, $\sigma_{i/o}$ are the stresses generated by inner and outer SMAs for flexion/extension motions.

to the PD controller. It generates the desired control effort u. Based on the sign of u, the relevant SMA (inner/outer) is activated for flexion/extension motion which generates stress accordingly $\sigma_{i/o}$. These stresses generate torques for the corresponding joint of robotic finger.

5 Experimental Results

Fig. 10 shows our experimental setup for the 3-DOF SMA finger mechanism. The SMA finger (1) is clamped with the bench vise. A temperature sensor (2) is attached to the SMA actuator to monitor its temperature. The amplifier and interface module MAX6675 K (3) are used to interface to the controller. Arduino Due (4) is used for data acquisition and PWM control signals for a host PC. First, we experimentally validate our finger mechanism applying a simple open-loop control method. As a result, experimentally achieved finger postures are illustrated in Fig. 11. Fig. 11 (a) shows the initial posture of the SMA finger where all actuators are off. In Fig. 11 (b), the SMA-1 actuator is activated to move the third link (distal). In Fig. 11 (c), the SMA-3 actuator is activated to move the second link (middle). In Fig. 11 (d), the SMA-5 actuator is activated to move the first link (proximal). Fig. 11 (e) shows the grasping pose while actuating all the inner SMA actuators (SMA-1, SMA-3, and SMA-5) simultaneously. In Fig. 11 (f, g, h) each link is restored to its extension position by activating the antagonistic SMA actuators (SMA-2, SMA-4, and SMA-6) respectively. The open-loop control of each pair of SMA actuators can change the corresponding joint from 0° from 90°. Hence we validated the open-loop control of all the SMA actuators in the SMA finger.

We then conducted experiments with closed loop control. An independent joint control strategy is developed using a simple proportional-derivative (PD) control method.The experimental setup for closed loop control is shown in

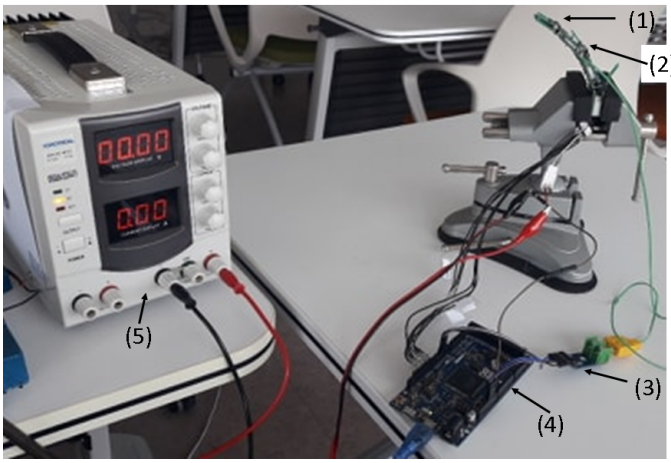

Fig. 10: Open loop control experimental setup of the 3-DOF SMA finger mechanism (1) The SMA Finger (2) A temperature sensor (3) Amplifier and interface module (4) Controller:Arduino Due.

Fig. 12, which include IMU sensors attached to each link and temperature sensors attached to each SMA actuator. The details of the controller design are described in Section 4.3. Since, the joint controller is identically used in all fingers joints and have similar regulation performance, we present only experimental results obtained for joint 3 (θ_3). The joint (θ_3) was actuated using two SMAs. These SMAs were attached in antagonistic configuration (for flexion and extension movement). In particular, for flexion, SMA-1 is used (which was attached on the inner side of finger). Whereas, for extension, SMA-2 is utilized (which was attached on the outer side of the finger).

Fig. 13 shows comparison of experimental and simulation results obtained for the joint 3 (θ_3). It shows the successful regulation of the desired angle for the step up. The response obtained from simulation and experiment is similar. The initial position of the θ_3 is at 7.5° and the desired angle is 20° to demonstrate flexion motion. For this motion, 3-DOF SMA finger used SMA-1 to produce the contraction forces. The robotic finger supplied current to the SMA-1 (13a) to generate the desired motion. So, SMA-1 gets heated (13c) and produced forces. Once, the finger reaches the desired angle, it turns off the SMA-1. However, if the finger acquired angle gets higher than the desired value, it fired SMA-2 to produce counter forces as shown in Fig. (13b) which causes the heating of SMA-2 as shown in Fig. 13c. Fig. 14 shows three poses at 0 sec, 2.8 sec and 5.2 sec.

In a similar way, in Fig. 15, we have compared the step down case for the joint 3 (i.e. θ_3). Results are similar for the step up case as shown in Fig. 13.

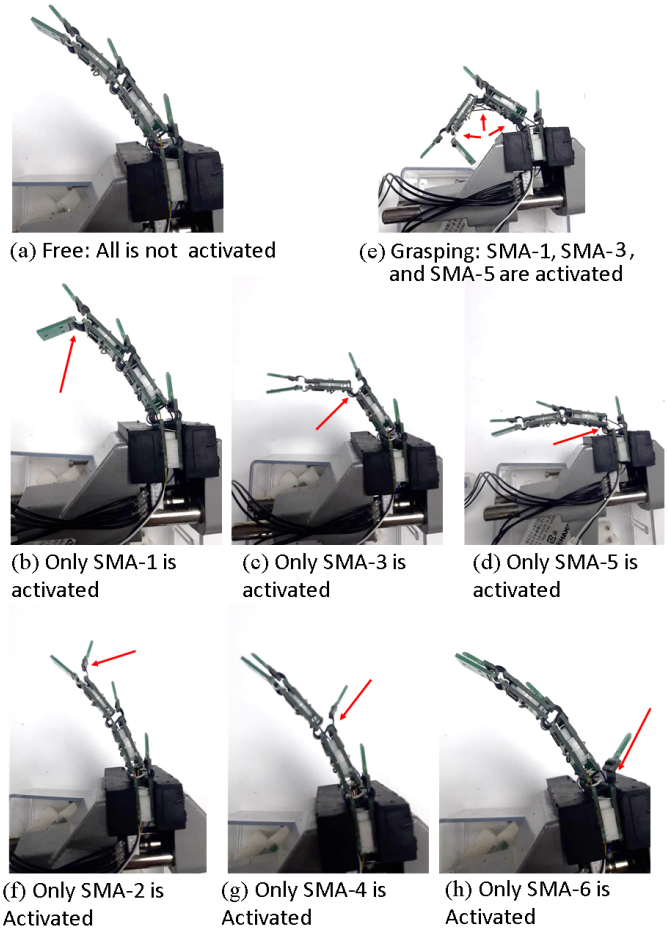

Fig. 11: Experimental validation of SMA finger postures applying a open- loop control method

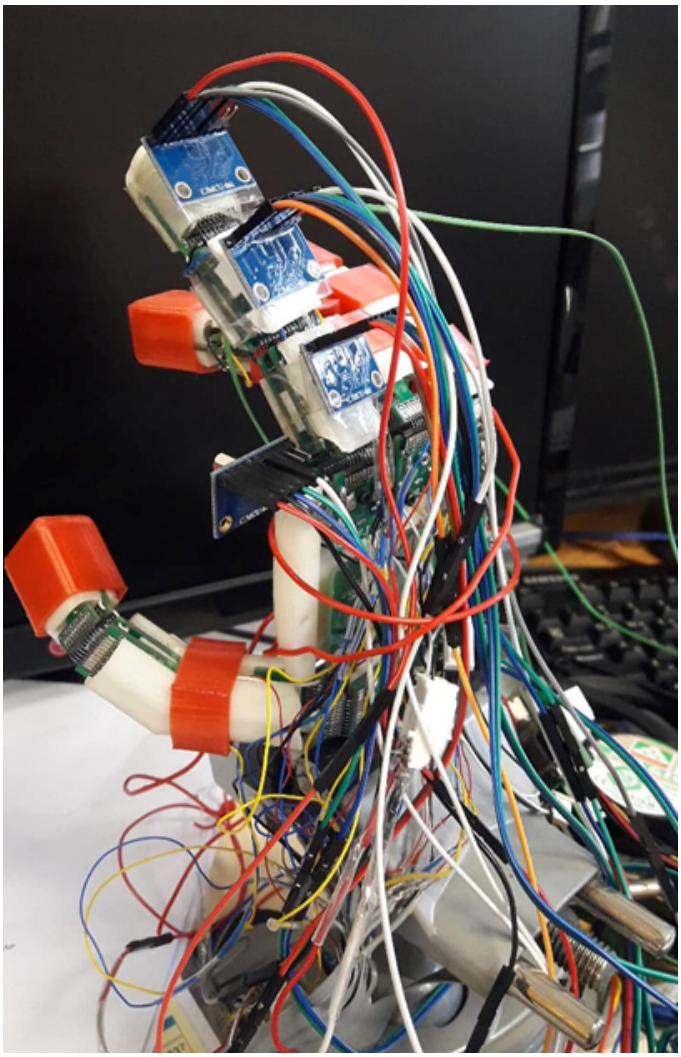

Fig. 12: Closed loop control experimental setup of the 3-DOF SMA finger mechanism

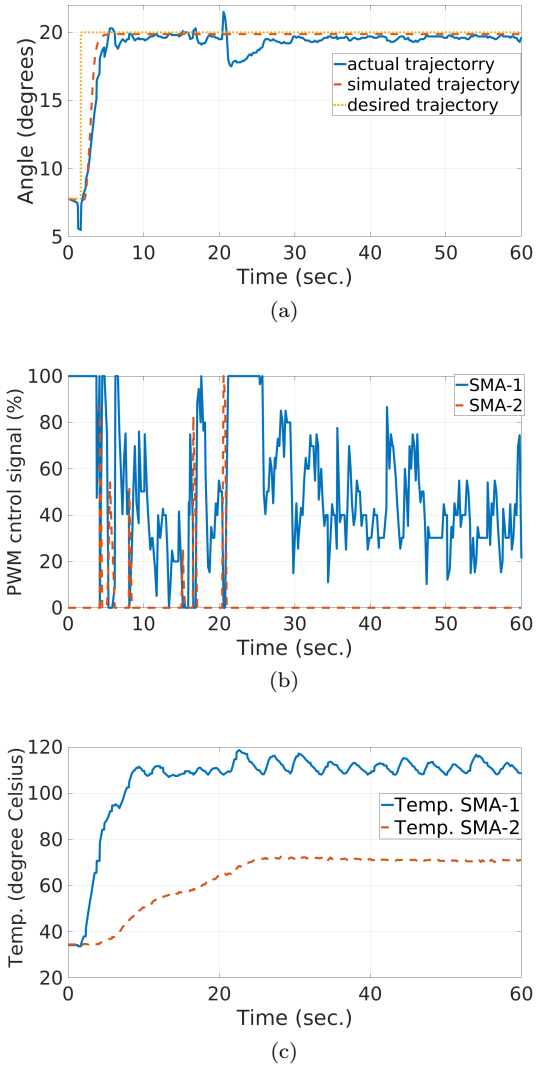

Fig. 13: Experimental evaluation of flexion motion in joint 3 (θ_3) of the SMA finger. (a) comparison of simulated and actual trajectory for step up case - starting from initial position 7.5° and reaching to the desired angle 20°, (b) the control signal in PWM percentage for SMA-1 (responsible for flexion movement) and SMA-2 (responsible for extension movement), and (c) change in temperature in SMA-1 and SMA-2 during the flexion motion.

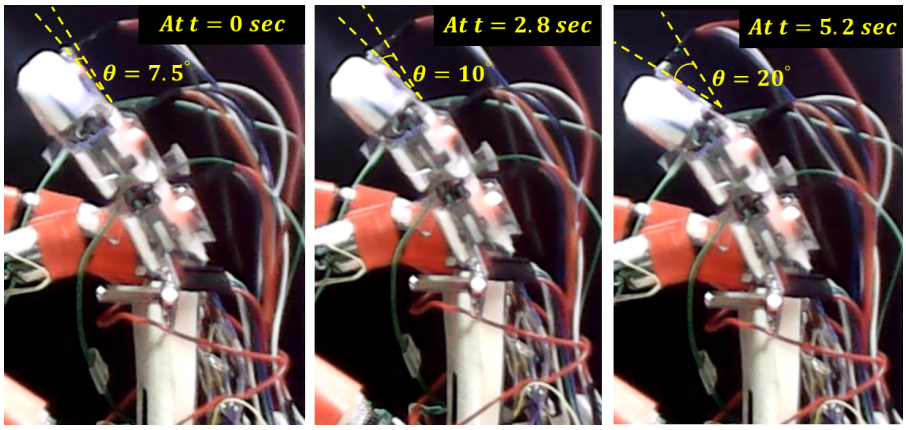

Fig. 14: Closed loop control experiment: 3 poses at 0 sec, 2.8 sec and 5.2 sec.

The experimental results in Figs. 13-15 shows the effectiveness of SMAs as actuators in biologically inspired finger mechanism. Using SMA, we designed light weight actuation mechanism. Furthermore, the closed loop proportional-derivative (PD) successfully tracked the desired angel for the required flexion/extension motion. The PD controller successfully generated the actuation signal to regulate the desired value. The main implications of these experimental results are that using this mechanism we can grasp the object softly using compliant motion. This motion was made possible due to the controlled behavior of SMAs as actuators.

6 Conclusion

In this research, we present a novel robotic finger mechanism which is composed of 3 links and 3 joints. Mechanical and thermal characterization of the SMA are established. This robotic finger is fabricated applying three bending SMA actuators and three antagonistic bending SMA actuator similar to a musculoskeletal structure of a human finger. The posture and motion of the finger are realized using coordinated control of each actuators. Independent joint control strategies for the robotic finger were experimentally verified by applying proportional-derivative (PD) method. Our experimental results confirm that joint angles of the SMA finger can be regulated to achieve the desired posture similar to human finger using a simple PD controller.

Acknowledgment

This work was supported by the National Research Foundation of Korea (NRF) grant funded by the Korea Government (MSIT) (No. 2017R1A2B4008056).

Also, the first and second authors are funded by the Korea Research Fellowship (KRF) program by the National Research Foundation (NRF) with KRF Grant (2019H1D3A1A01071124) and (2019H1D3A1A01102998), respectively.

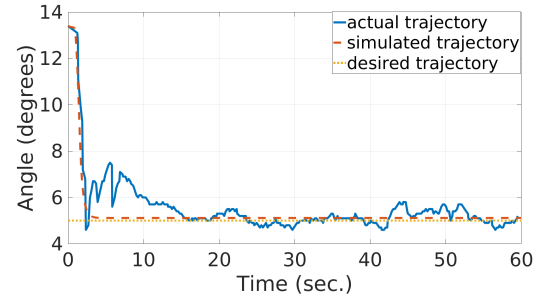

(a)

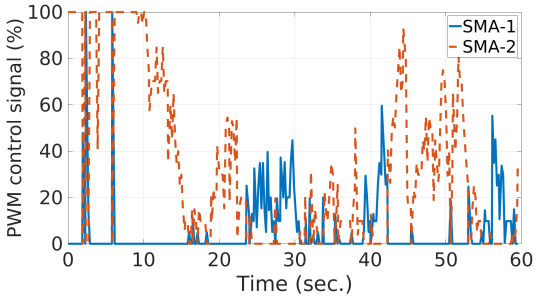

(b)

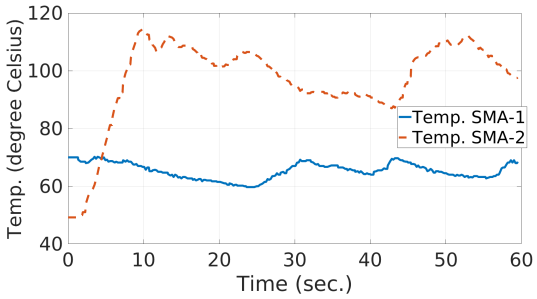

(c)

Fig. 15: Experimental evaluation of extension motion in joint 3 (θ_3) of SMA finger. (a) comparison of simulated and actual trajectory for the step down case - starting from initial position 13.4° and reaching to the desired angle 5°, (b) control signal in PWM percentage for SMA-1 (responsible for flexion movement) and SMA-2 (responsible for extension movement), and (c) change in temperature in SMA-1 and SMA-2 during the extension motion.

References

Ades C, Dilibal S, Engeberg E (2020) Shape memory alloy tube actuators inherently enable internal fluidic cooling for a robotic finger under force control. Smart Materials and Structures

Ali HF, Baek H, Jang T, Kim Y (2020) Finger-like mechanism using bending shape memory alloys. In: ASME 2020 29th Conference on Information Storage and Processing Systems, American Society of Mechanical Engineers Digital Collection

Almubarak Y, Punnoose M, Maly NX, Hamidi A, Tadesse Y (2020) Kryptojelly: A jellyfish robot with confined, adjustable pre-stress, and easily replaceable shape memory alloy niti actuators. Smart Materials and Structures

Andrianesis K, Tzes A (2015) Development and control of a multifunctional prosthetic hand with shape memory alloy actuators. Journal of Intelligent & Robotic Systems 78(2):257–289

Brinson LC (1993) One-dimensional constitutive behavior of shape memory alloys: thermomechanical derivation with non-constant material functions and redefined martensite internal variable. Journal of intelligent material systems and structures 4(2):229–242

Bundhoo V, Haslam E, Birch B, Park EJ (2009) A shape memory alloy-based tendon-driven actuation system for biomimetic artificial fingers, part i: design and evaluation. Robotica 27(1):131

DeLaurentis K, Mavroidis C, Pfeiffer C (2000) Development of a shape memory alloy actuated robotic hand. In: Proc. ACTUATOR: 7th International Conference on New Actuators, pp 281–284

Elahinia MH, Ahmadian M (2005) An enhanced sma phenomenological model: I. the shortcomings of the existing models. Smart materials and structures 14(6):1297

Gilardi G, Haslam E, Bundhoo V, Park EJ (2010) A shape memory alloy based tendon-driven actuation system for biomimetic artificial fingers, part ii: modelling and control. Robotica 28(5):675–687

Jani JM, Leary M, Subic A, Gibson MA (2014) A review of shape memory alloy research, applications and opportunities. Materials & Design (1980-2015) 56:1078–1113

Langbein S (2009) Development of standardised and integrated shape memory components in "one-module"-design. In: European Symposium on Martensitic Transformations, EDP Sciences, p 07010

Laurentis KJD, Mavroidis C (2002) Mechanical design of a shape memory alloy actuated prosthetic hand. Technology and Health Care 10(2):91–106

Lee JH, Chung YS, Rodrigue H (2019a) Long shape memory alloy tendon-based soft robotic actuators and implementation as a soft gripper. Scientific reports 9(1):1–12

Lee JH, Chung YS, Rodrigue H (2019b) Long shape memory alloy tendon-based soft robotic actuators and implementation as a soft gripper. Scientific reports 9(1):1–12

Liang C, Rogers CA (1997) One-dimensional thermomechanical constitutive relations for shape memory materials. Journal of intelligent material systems and structures 8(4):285–302

Liu M, Hao L, Zhang W, Zhao Z (2020) A novel design of shape-memory alloy-based soft robotic gripper with variable stiffness. International Journal of Advanced Robotic Systems 17(1):1729881420907813

Lu Y, Xie Z, Wang J, Yue H, Wu M, Liu Y (2019) A novel design of a parallel gripper actuated by a large-stroke shape memory alloy actuator. International Journal of Mechanical Sciences 159:74–80

Maffiodo D, Raparelli T (2019) Flexible fingers based on shape memory alloy actuated modules. Machines 7(2):40

Mao T, Peng H, Lu X, Zhao C (2019) A small locust inspired actuator driven by shape memory alloys and piezoelectric strips. Smart Materials and Structures 28(10):105051

Peng H, Mao T, Lu X (2020) A small legged deformable robot with multi-mode motion. Journal of Intelligent Material Systems and Structures 31(5):704–718

Rodrigue H, Wang W, Kim DR, Ahn SH (2017) Curved shape memory alloy-based soft actuators and application to soft gripper. Composite Structures 176:398–406

Simone F, Rizzello G, Seelecke S (2017) Metal muscles and nerves—a self-sensing sma-actuated hand concept. Smart Materials and Structures 26(9):095007

Simone F, Rizzello G, Seelecke S, Borreggine S, Naso D (2019) Modeling and identification of a shape memory alloy robotic finger actuator. In: 2019 18th European Control Conference (ECC), IEEE, pp 1097–1102

Song SH, Kim MS, Rodrigue H, Lee JY, Shim JE, Kim MC, Chu WS, Ahn SH (2016) Turtle mimetic soft robot with two swimming gaits. Bioinspiration & biomimetics 11(3):036010

Tai K, El-Sayed AR, Shahriari M, Biglarbegian M, Mahmud S (2016) State of the art robotic grippers and applications. Robotics 5(2):11

Tanaka K (1986) A thermomechanical sketch of shape memory effect: one-dimensional tensile behavior. RES MECHANICA

Wang W, Ahn SH (2017) Shape memory alloy-based soft gripper with variable stiffness for compliant and effective grasping. Soft robotics 4(4):379–389

Wang W, Rodrigue H, Kim HI, Han MW, Ahn SH (2016) Soft composite hinge actuator and application to compliant robotic gripper. Composites Part B: Engineering 98:397–405

Wang W, Yu CY, Abrego Serrano PA, Ahn SH (2020a) Shape memory alloy-based soft finger with changeable bending length using targeted variable stiffness. Soft robotics 7(3):283–291

Wang Y, Zheng S, Song Z, Pang J, Li J (2020b) A coupling dynamic model for studying the physical interaction between a finger exoskeleton and a human finger. IEEE Access 8:125412–125422